CEIG - Spanish Computer Graphics Conference (2016)
Alejandro García-Alonso and Belen Masia (Editors)

Characterisation of Position Based Dynamics for Elastic Materials

C. Rodero[1], P. Real[1], P. Zuñeda[2], C. Monteagudo[2], M. Lozano[3] and I. García-Fernández[3]

[1]Facultat de Matemàtiques, Universitat de València, Spain
[2]Escola Tècnica Superior d'Enginyeria, Universitat de València, Spain
[3]Departament d'Informàtica, Universitat de València, Spain

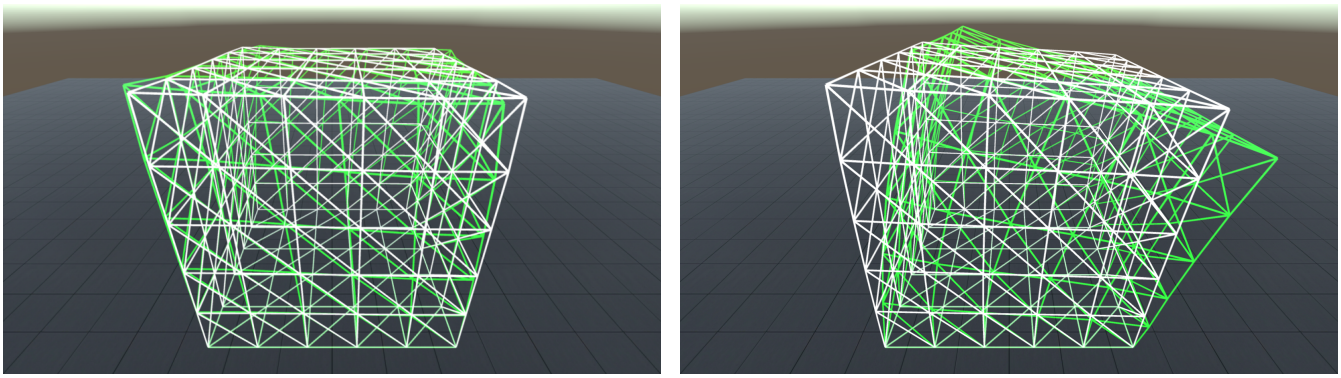

Figure 1: *Comparison between a $5 \times 5 \times 5$ PBD hexahedral mesh, fitted with the proposed method, and the reference FEM mesh for $E = 100$ and $\nu = 0.2$. The figures correspond to torsion (left) and shear (right) deformation tests. Green mesh corresponds to PBD and white mesh to FEM.*

Abstract

Position Based Dynamics (PBD) methodology is a widely used approach for simulation of deformable bodies in the context of video games. Its main advantages over force based methods are its unconditional stability and its constraint based approach. However, it does not involve physically inspired parameters and its behaviour depends on time step size. This makes it difficult to reproduce a given elastic behaviour. In this work we perform an analysis of the mechanical properties in a PBD elastic system, and compare it to the Finite Element Method (FEM). We propose a methodology to fit the parameters of PBD to simulate a particular Young's modulus and Poisson's ratio.

Categories and Subject Descriptors (according to ACM CCS): I.3.7 [Computer Graphics]: Three-Dimensional Graphics and Realism—Virtual Reality

1. Introduction

Computer animation and simulation of deformable materials in interactive applications is commonly addressed using Mass-Spring meshes or shape matching techniques. Although Finite Element Method simulation has been used also for interactive applications (see Müller and Gross [MG04]), it has efficiency limitations specially when it comes to topology changes in the simulated objects. More recently, the Position Based Dynamics (PBD) methodology is gaining popularity thanks to its unconditional stability and currently it is a widely used technique in video games.

However, these methods (Mass-Spring, Shape-Matching and Position Based models) are only physically inspired and they have parameter sets that do not correspond to the standard parameters in elasticity, namely Young's modulus (the relationship between stress and strain in a material) and Poisson's ratio (the negative ratio of transverse to axial strain).

Several works have faced the problem of parameter fitting for Mass-Spring models. However, the mechanical properties of Position Based Dynamics models have not been studied systematically. A characterisation of the dynamics of the Position Based Dynamics elasticity model would determine to what extent it is capable of reproducing actual elastic materials. In this paper we conduct

DOI: 10.2312/ceig.20161314

an analysis of an elastic hexahedral element simulated with PBD under small deformations.

The main contribution of our paper is a procedure to fit its parameters with the goal of reproducing a given elastic behaviour. Our method starts with a Finite Element linear elastic model, with known Young's modulus and Poisson's ratio. We perform a numerical linearisation of a general PBD system and pose an optimisation problem to determine its parameters. The procedure, described in Section 3, is independent on the geometry of the system or the type of constraints used. Then, the method is applied to a cubical PBD system in Section 4. The method is tested in several scenarios to evaluate the methodology and the resulting approximation of an elastic material. Figure 1 shows a comparison between an hexahedral PBD mesh, fitted with the proposed method, and the reference FEM mesh under torsion and shear deformation.

2. Related work

Position Based Dynamics [MHHR06] has been introduced as an stable methodology for the simulation of elastic materials. A PBD model consists of a particle system, where each particle is characterised by its location $\mathbf{p}_i$ and velocity $\mathbf{v}_i$, and a set of constraints on the locations $C_j(\mathbf{p}_1,\dots,\mathbf{p}_n) = 0$. Simulation is performed in a predictor-corrector fashion. First external and mass forces are applied to the particles through a numerical integration step. This is called the prediction step. Then, the locations of all the particles are projected into a state where the constraints are met in what is called the correction step. Velocities are updated to be consistent with the final location change.

If we denote the vector containing all particle locations as $\mathbf{p} = (\mathbf{p}_1,\dots,\mathbf{p}_n)$, then for a given constraint $C(\mathbf{p})$, the projection of particle i is given by

$$\Delta\mathbf{p}_i = -k\frac{C(\mathbf{p})}{\sum_j w_j\|\nabla_{\mathbf{p}_j}C(\mathbf{p})\|^2}w_i\nabla_{\mathbf{p}_i}C(\mathbf{p}) \tag{1}$$

where $\nabla_{\mathbf{p}_i}C(\mathbf{p})$ is the jacobian matrix of C with respect to the components of $\mathbf{p}_i$; $0 \le k \le 1$ is a correction factor that modulates the amount of projection actually applied and $w_i = 1/m_i$ where m_i is the mass of the particle i. This latter parameter is defined in order to help to create unmovable particles by setting $w_i = 0$. The projection is applied per constraint, in an iterative process. By adjusting k, and the number of projection iterations, this approach can be used to simulate elastic materials. Further details on the methodology and different applications can be found in [MHHR06, BMO*14].

This methodology, however, has the limitation that elasticity is controlled by two non-physical parameters; the correction or stiffness factor k and the number of projection iterations. Recently Bender et al. [BKCW14] have introduced a set of energy constraints for the simulation of continuous materials, including elastic deformations, where physically meaningful parameters are used. However, to the best of our knowledge no previous work has been conducted in order to analyse the mechanical properties of PBD elastic materials based on geometric constraints.

This problem is analogous to parameter fitting in modelling methodologies such as Mass-Spring Models (MSM). In MSM, a deformable object is discretised as a particle system, and the objects structure is represented by a set of springs that link them. The evolution of the system is computed using Second Newton's Law. Although MSM are physically inspired, there is not a direct translation from the stiffness constants of the set of springs to the mechanical parameters of an elastic material, and several authors have addressed the problem of parameter fitting. We review the main efforts in this direction, since the proposed methodologies can be applied to the equivalent problem for PBD. Following the classification proposed in [LSH07] and in [SVAC12] we can consider data driven approaches and analytical approaches.

Data driven approaches use a set of reference deformations, and rely on different optimisation methods to find the parameters for the MSM. Typically the function to optimise is some error measure of the deformation of a simulated MSM, compared to the reference deformation samples. It has been observed the existence of local minima, which has led to the use of strategies such as simulated annealing [DKT95] or evolutionary algorithms [LPC95, NNUF04, BSSH04, ZGF07].

Analytical approaches try to develop expressions that involve both the Mass-Spring parameters and the elastic parameters describing a deformable material. Van Gelder [Gel98] linearised the system of equations of the MSM to find that, in general, its stiffness matrix cannot be directly equated to a linear FEM stiffness matrix. More recently, Lloyd et al. [LSH07] derive analytic expressions for triangular (for 2D) and tetrahedral (for 3D) Mass-Spring elements and find that a closed form solution can only be found on equilateral triangles. Other authors develop analytical expressions for the spring stiffness under certain particular deformations, to fit the parameters that best reproduce such deformations [MBT03, BBJ*09]. San Vicente et al. [SVAC12] follow this approach and use the derived analytical expressions to fit the parameters using data from uniaxial tensile deformations.

Some works, further than fitting the MSM parameters to fit a certain behaviour, provide a more in depth analysis of the dynamics of a general MSM model. The work by San Vicente et al. [SV11, SVAC12] compute the elastic properties and parameters for an hexahedral Mass-Spring system, while Kot et al. [KNS15] develop on their methodology to characterise the dynamics of an arbitrary triangular Mass-Spring mesh.

In our work, we shall follow the approach by Van Gelder [Gel98] and by Lloyd et al. [LSH07] to fit a linearisation of a PBD stiffness matrix. Our error function is based on that of [LSH07], measuring the difference between the PBD stiffness matrix and a linear FEM stiffness matrix in Frobenius norm. The main difference is that we compute the stiffness matrix numerically by finite differences. We shall use an hexahedral PBD system formed by 8 particles, as it is done for MSM in [MBT03, SVAC12]. In our case, however, we explicitly consider volume preservation during parameter fitting.

3. Elasticity in Position Based Dynamics

Elasticity theory studies the relationship between forces applied on a body and the reversible deformation of the body. Constitutive models are often expressed as a relationship between strain ε, as a measure of deformation, and stress σ, which is force per unit area.

In linear elasticity, this relationship is of the form

$$\sigma = \mathbf{D}\varepsilon \tag{2}$$

where D expresses the elastic properties of the material. For isotropic materials the stress-strain relation in Equation 2 is called Saint Venant-Kirchhoff model.

The Finite Element Modelling (FEM) methodology uses a discretisation of this model to turn it into a system of linear equations. If we consider an hexahedral portion of elastic material, or hexahedral *element*, its state is described by the location if its eight vertexes or *nodes*. An element with the ordered vertexes and axes as is commonly found in the literature (see for example [Zie77]) is shown in Figure 2. In absence of deformation, node i has a position $\mathbf{x}_i$. If the system is deformed, with a nodal deformation $\mathbf{u}_i$ for node i, then, the position of every node will be $\bar{\mathbf{x}}_i = \mathbf{x}_i + \mathbf{u}_i$. By means of the Finite Element Modelling (FEM), this relationship can be turn into a relationship between nodal deformations and generalised nodal forces $\mathbf{f}_i$.

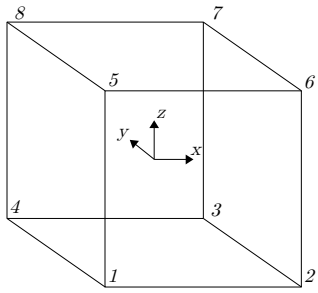

Figure 2: *A FEM hexahderal element.*

We consider the vectors $\mathbf{f} = (\mathbf{f}_1, \ldots, \mathbf{f}_8)^T$ and $\mathbf{u} = (\mathbf{u}_1, \ldots, \mathbf{u}_8)^T$. Then, the FEM formulation defines a matrix $\mathbf{K}^{\text{FEM}}$ for which

$$\mathbf{f} = \mathbf{K}^{\text{FEM}}\mathbf{u}, \tag{3}$$

where $\mathbf{f}$ is the applied force and $\mathbf{u}$ is the deformation of the system in static equilibrium. The FEM stiffness matrix for an element has the form

$$\mathbf{K}^{\text{FEM}} = \int_V \mathbf{B}^T \mathbf{D}\mathbf{B}\, dV$$

where V is the volume of the element, matrix $\mathbf{B}$ includes partial derivatives of the interpolation functions in the element and matrix $\mathbf{D}$ is the aforementioned matrix which defines the relationship between strain and stress, given by

$$\mathbf{D} = A \begin{bmatrix} 1-\nu & \nu & \nu & 0 & 0 & 0 \\ \nu & 1-\nu & \nu & 0 & 0 & 0 \\ \nu & \nu & 1-\nu & 0 & 0 & 0 \\ 0 & 0 & 0 & 1-2\nu & 0 & 0 \\ 0 & 0 & 0 & 0 & 1-2\nu & 0 \\ 0 & 0 & 0 & 0 & 0 & 1-2\nu \end{bmatrix} \tag{4}$$

where

$$A = \frac{E}{(1+\nu)(1-2\nu)} \tag{5}$$

being E the Young's modulus and ν the Poisson's ratio.

We have computed these integrals using the `integrate` instruction of the `SymPy` library in Python. `SymPy` currently uses a simplified version of the Risch algorithm [Ris69], called the Risch-Norman algorithm [NM77]. For non-elementary definite integrals, `SymPy` uses so-called Meijer G-functions (the most accepted definition can be found in [EB53]).

Now, let's consider an equivalent cubic portion of material, simulated with Position Based Dynamics. We build it by means of eight particles, placed at the vertexes of the cube and we define one or more constraints that describe the equilibrium state of the cube. If we linearise the dynamics of the system, we can find an equivalent to the stiffness matrix. We are seeking for a matrix $\mathbf{K}^{\text{PBD}}$ for which, when applying a force $\mathbf{f} = (\mathbf{f}_1, \ldots, \mathbf{f}_8)^T$ to the PBD particles,

$$\mathbf{f} = \mathbf{K}^{\text{PBD}}\mathbf{u} \tag{6}$$

with small $\mathbf{u}$. In practice, to use the dependence of $\mathbf{u}$ as a function of $\mathbf{f}$ is not the most convenient approach, since it involves the inverse of $\mathbf{K}^{\text{PBD}}$. Instead, we shall consider $\mathbf{f}$ as a function of $\mathbf{u}$. However, this poses a difficulty, because the output of the PBD projection process is not a force or an acceleration, but a position change.

To overcome this we shall calculate the force that is equivalent to the PBD projection, $\Delta\mathbf{p}$. We mean a force that, when integrated numerically, causes the same change in position than a given $\Delta\mathbf{p}$. When using semi-implicit Euler scheme with a time step Δt, this force is given by

$$\mathbf{f}_i = \frac{m_i}{\Delta t^2}\Delta\mathbf{p}_i, \tag{7}$$

This strategy presents an additional advantage. The dynamics of the PBD method is known to be dependent on the size of the time step. By considering this equivalent force we shall include this dependence in our computation of the PBD parameters, as we shall see.

Thus, we consider $\Delta\mathbf{p}$ as a function that depends on the deformation $\mathbf{u}$ as defined previously. If we linearise this function near $\mathbf{u} = 0$, we have that, for small values of $\mathbf{u}$

$$\Delta\mathbf{p}(\mathbf{u}) \simeq \frac{\partial\Delta\mathbf{p}(0)}{\partial\mathbf{u}}\mathbf{u}, \tag{8}$$

and, using (7), we can define the stiffness matrix for PBD as

$$\mathbf{K}^{\text{PBD}} = \frac{\mathbf{M}}{\Delta t^2}\frac{\partial\Delta\mathbf{p}(0)}{\partial\mathbf{u}}. \tag{9}$$

where $\mathbf{M}$ is the mass matrix of the PBD system.

In a procedure analogous to FEM matrix assembly, the PBD stiffness matrix can be defined per constraint, and the stiffness matrix of the whole system is assembled by adding all the constraint stiffness matrices. This computation can be done analytically for some constraints, such as the distance constraint proposed in [MHHR06], while for others it can be hard to find a closed expression for $\mathbf{K}^{\text{PBD}}$.

At this point, it is important to remark a property of the original PBD method [MHHR06]; during a PBD iteration, the correction of the constraint applied in the first place is considered to compute the correction of subsequent constraints, using what they call a Gauss-Seidel-like scheme. However, our approach assumes that the corrections of all constraints are using the state of the system in the

previous time step. As a consequence, the previous development is implicitly assuming that the iterative projection process of PBD is done following a Jacobi-like scheme, as described by Macklin et al. [MMCK14]. If a Gauss-Seidel-like scheme is desired, the PBD stiffness matrix could be obtained from a sample of randomly ordered iterations.

3.1. Stiffness matrix fitting

In PBD there are two main controllable parameters associated to the method; the number of projection iterations, which is a global parameter, and a stiffness-like parameter $0 \leq k \leq 1$, which can be different for every constraint. In this work we shall consider a single iteration for our analysis, and consider the stiffness matrix as a function of the different $k_j,\ j = 1,\ldots,m$, for a system with m constraints. The extension of the methodology to a variable number of iterations is not difficult, but exceeds the scope of this paper.

Our main objective is to fit a set of PBD parameters which lead to an elastic behaviour consistent with given Young's modulus and Poisson's ratio. As the reference for a proper elastic behaviour we shall consider a FEM model with the nodes located at the same positions of the PBD particles. Following the approach by Lloyd et al. [LSH07], we will use an optimisation method to find the values of the k_j which minimise the difference between $\mathbf{K}^{\text{PBD}}$ and $\mathbf{K}^{\text{FEM}}$, where the PBD matrix is considered as a function of the stiffness parameters $\mathbf{K}^{\text{PBD}} = \mathbf{K}^{\text{PBD}}(k_1,\ldots,k_m)$.

This optimisation has an additional difficulty; the FEM stiffness matrix can have an arbitrarily large norm, since E is not upper bounded, and the dividing term $1-2\nu$ tends to infinity as ν tends to $\frac{1}{2}$. On the contrary, a convergent PBD projection needs to be a contractive iteration and, as a consequence, the Jacobian of the PBD projection with respect to the state of the system, $\partial\Delta\mathbf{p}/\partial\mathbf{u}$ has a bounded norm.

From Equation (9) we see that the only term that is not bounded in our definition of $\mathbf{K}^{\text{PBD}}$ is the fraction $1/\Delta t^2$. This implies that, when a particular elastic material is to be reproduced using PBD, the integration time step cannot be freely chosen. Taking this into account, we propose to set the value of Δt as

$$\Delta t = \sqrt{\frac{\|\mathbf{M}\|}{\|\mathbf{K}^{\text{FEM}}\|}}, \tag{10}$$

since this value, when applied in (9), will enable arbitrarily large norms for $\mathbf{K}^{\text{PBD}}$. From this value or Δt, we use the following optimisation problem to fit the PBD parameters:

$$(k_1,\ldots,k_m) = \arg\min_{k_i}\left\{\left\|\mathbf{K}^{\text{FEM}} - \frac{\mathbf{M}}{\Delta t^2}\frac{\partial\Delta\mathbf{p}}{\partial\mathbf{u}}(k_1,\ldots,k_m)\right\|\right\} \tag{11}$$

subject to the constraints $0 \leq k_j \leq 1$. Here the norm used is the Frobenius norm, as proposed by [LSH07]. For solving the optimisation problem we have used MatLab's instruction `fminsearch`, a command that uses the Nelder-Mead simplex algorithm as described in Lagarias et al. [LRWW98].

The previous methodology to fit the parameters of the PBD system can be summarised as follows:

1. Choose a Young's modulus E and a Poisson's ratio ν.
2. Build a reference PBD system and an equivalent FEM element.
3. Build the FEM matrix, and set Δt.
4. Fit the PBD parameters solving the optimisation problem (11).

The last step can be done either analytical or numerically, depending on the complexity of the resulting PBD matrix.

4. Cubic PBD element

To validate the proposed methodology we follow the proposal by San Vicente et al. [SVAC12] and use an hexahedral FEM element to fit a cubic PBD system formed by eight masses. In the PBD system, we use distance constraints where [SVAC12] use springs and, as in their work, the constraints can be classified in three types; edge constraints, which link masses connected by an edge of the cube; face constraints, which link particles through the diagonal of a face; and internal diagonal constraints, which link particles that have not been linked by any of the previous constraints. All the constraints of the same type will share a unique stiffness coefficient.

The distance constraint proposed by [MHHR06] is given by

$$C(\mathbf{p}_i,\mathbf{p}_j) = \|\mathbf{p}_i - \mathbf{p}_j\| - d$$

where d is the rest distance. For this constraint, the projection is given by [MHHR06]

$$\Delta\mathbf{p}_i = -\frac{w_i}{w_j}\Delta\mathbf{p}_j = \frac{w_i}{w_i+w_j}\left(\|\mathbf{p}_{ij}\| - d_{ij}\right)\frac{\mathbf{p}_{ij}}{\|\mathbf{p}_{ij}\|} \tag{12}$$

where $\mathbf{p}_{ij} = \mathbf{p}_i - \mathbf{p}_j$.

Using a single iteration step, the stiffness matrix for this constraint has the same analytical form as the equivalent stiffness matrix for a Mass-Spring Model developed by Lloyd et al. [LSH07]. But in their work it is shown that the resulting matrix cannot be equated to $\mathbf{K}^{\text{FEM}}$ except for the case of an equilateral triangle of springs. Moreover, although the internal diagonal constraints contribute to volume preservation, they are also coupled with other deformation modes. For these reasons we add to the distance constraints the volume preservation constraint proposed by [MHHR06]. Although volume preservation potentials have been defined for MSM models [THMG04], in the parameter fitting literature this kind of forces are not usually included.

For closed triangle meshes, volume preservation can be enforced by means of a constraint as seen in [MHHR06]. We add an equality constraint concerning all 8 nodes of the mesh with constraint function

$$C(\mathbf{p}_1,\ldots,\mathbf{p}_8) = \left(\sum_{i=1}^{N_{\text{triangles}}}\left(\mathbf{p}_{t_1^i}\times\mathbf{p}_{t_2^i}\right)\cdot\mathbf{p}_{t_3^i}\right) - V_0$$

where V_0 is the volume of the undeformed cube. Here t_1^i, t_2^i and t_3^i are the three indexes of the vertexes belonging to triangle i. The sum computes the actual volume of the closed mesh. This constraint function yields the gradients

$$\nabla_{\mathbf{p}_i}C = \sum_{j:t_1^j=i}\left(\mathbf{p}_{t_2^j}\times\mathbf{p}_{t_3^j}\right) + \sum_{j:t_2^j=i}\left(\mathbf{p}_{t_3^j}\times\mathbf{p}_{t_1^j}\right) + \sum_{j:t_3^j=i}\left(\mathbf{p}_{t_1^j}\times\mathbf{p}_{t_2^j}\right)$$

The inclusion of this constraint has the drawback that it does not have a tractable expression for its jacobian matrix, necessary to

build the stiffness matrix defined in Equation (9). Instead, we shall compute the matrix of the elastic PBD cube numerically using finite differences.

Since all the distance constraints of the same type share the same stiffness coefficient, we have a PBD system with four parameters: the stiffness of edge constraints, k_e; the stiffness of face constraints, k_f; the stiffness of internal diagonal constraints, k_d; and the stiffness of the volume preservation constraint, k_v.

5. Results

To show the proposed methodology and evaluate the results we have computed the values of the PBD parameters for the range of positive values of the Poisson's ratio, $\nu \in [0, \frac{1}{2})$. Since the linear FEM stiffness matrix depends linearly on E, as it can be deduced from equations (4) and (5), the results are independent on its value. For this reason in this section all the results are shown only for $E = 1$.

We present three main sections. In the first place we show the results of parameter fitting for the PBD constants. Next, we present the results of deformation tests on the eight node cube, and the error measured against the same scenario simulated using linear FEM. Finally, we simulate equivalent scenarios using an elastic cube formed by an hexahedral mesh.

5.1. Parameter fitting

We have solved the optimisation problem for a series of values of ν in the range 0 to $\frac{1}{2}$, and a Young's modulus $E = 1$. For each value of ν, the relative error

$$e_r = \frac{\|\mathbf{K}^{\text{PBD}} - \mathbf{K}^{\text{FEM}}\|}{\|\mathbf{K}^{\text{FEM}}\|} \tag{13}$$

has been computed. One of the differences between our PBD elastic cube and the Mass-Spring Models that have been analysed in the context of parameter fitting is the introduction of the volume constraint. To determine the relevance of this constraint in the results we have repeated the parameter adjustment forcing $k_v = 0$. In Figure 3 the values of the fitted stiffness coefficients are presented.

The upper figure shows the values for the fitting considering all four stiffness constants, while the lower figure shows the results when the volume constraint is not considered, by forcing $k_v = 0$. From the results it is clear that from $\nu = 0.29$ the stiffness k_v gains relevance, approaching $k_v = 1$ as ν tends to $\frac{1}{2}$. On the contrary, the value of k_d reduces to approach zero in the same range. In the fitting without volume constraint, we also observe this reduction in the value of the constants, but it does not approach $k_d = 0$. Looking at the form of the plots in (5.1) we have decided to make a polynomial fitting. We adjust de data by two polynomials of second order in

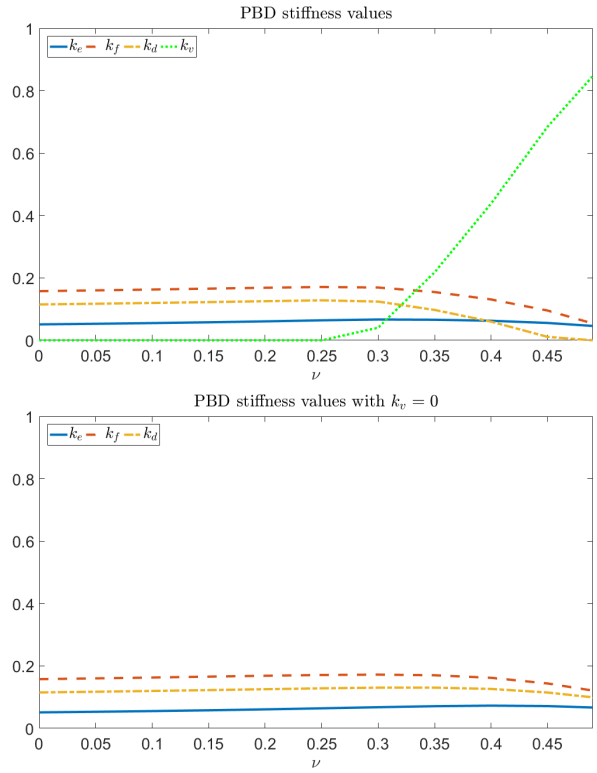

Figure 3: *Parameter values obtained for the PBD cubic element for different values of Poisson's ratio ν. The values are shown for the problem with all four constraint types (top) and forcing the volume preservation constraint to be $k_v = 0$ (bottom).*

each case, when $\nu \leq 0.29$ and when $\nu \geq 0.29$.

$$k_e(\nu) = \begin{cases} 0.0698\nu^2 + 0.0343\nu + 0.0511 & 0 \leq \nu \leq 0.29 \\ -0.7204\nu^2 + 0.4656\nu - 0.0084 & 0.29 \leq \nu < 0.5 \end{cases}$$

$$k_f(\nu) = \begin{cases} -0.0302\nu^2 + 0.0614\nu + 0.1572 & 0 \leq \nu \leq 0.29 \\ -2.3822\nu^2 + 1.2909\nu - 0.0044 & 0.29 \leq \nu < 0.5 \end{cases}$$

$$k_d(\nu) = \begin{cases} 0.0527\nu + 0.1147 & 0 \leq \nu \leq 0.29 \\ -0.5795\nu^2 - 0.2818\nu + 0.2636 & 0.29 \leq \nu < 0.5 \end{cases}$$

In the case of k_v we have approximated the data by a third degree polynomial for $\nu \geq 0.29$. The fitted polynomial is

$$k_v(\nu) = -50.6270\nu^3 + 63.1461\nu^2 - 21.4563\nu + 2.1615$$

and $k_v = 0$ if $\nu \leq 0.29$. Figure 4 shows the graph of the polynomial regression compared with the fitted parameters.

The observed behaviour of the stiffness coefficients indicates that the volume constraint plays a relevant role to get a better model fitting. This analysis is confirmed by the relative error value of the approximation, shown in Figure 5. The relative error in both fitting problems is the same until a value for the Poisson's ratio $\nu \simeq 0.29$. But the results show that from that value of ν the error increases if

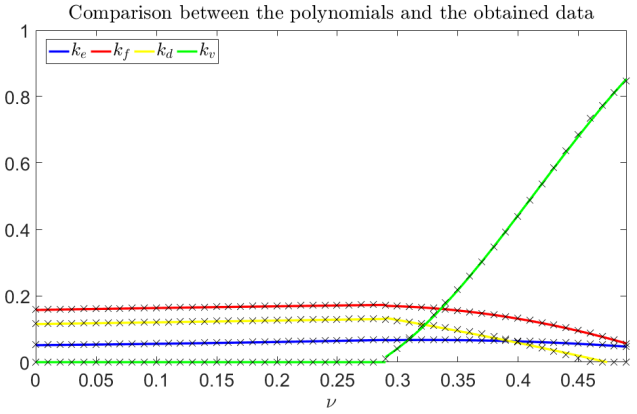

Figure 4: *Comparison between the previously obtained polynomials and the data from the minimisation strategy. The polynomials are represented with a line, while the fitted data are represented with crosses.*

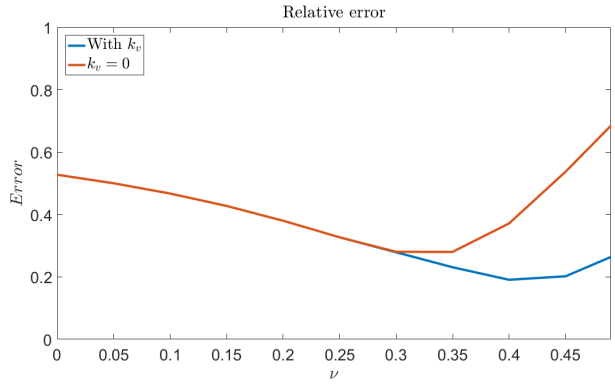

Figure 5: *The fitting relative error for the optimal parameter values for different values of* ν. *The errors for the complete set of parameters and for the model without volume constraint are shown.*

the volume constraint is not considered, and becomes higher as the Poisson's ratio approaches its upper limit.

Another conclusion that can be taken from the figure is that the relative error of the cubic PBD element including volume constraint is always in values over 20%. Indeed, the error is higher when volume preservation is less relevant. These values indicate that it is not possible a very good fitting using this objective function and advise in favour of other error measures, such as the error in deformation tests, as proposed by San Vicente et al. [SVAC12].

5.2. Deformation test scenarios

To determine if the obtained values of the PBD parameters provide good simulation results, we have used three standard scenarios to test the behaviour of a single cubical PBD system compared to the equivalent cubical FEM element. We have fixed the four particles/nodes at the base of the cube (those with lower z coordinate), and have applied forces on the upper particles/nodes to induce small deformations. We have simulated a torsional deformation test, a shear deformation test and a longitudinal deformation test by traction. Figure 6 shows three cubes with deformations corresponding to these tests.

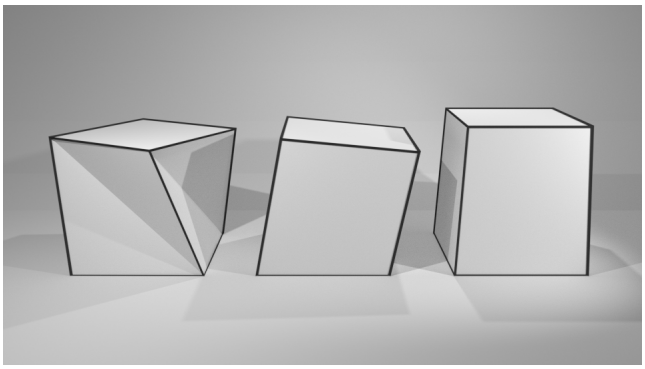

Figure 6: *Sample deformation tests used to evaluate the parameter fitting. From left to right, torsion along z axis, shear in the x direction and vertical traction in the positive z direction.*

The tests simulate static deformation. In the FEM model, deformation is obtained from forces by solving equation (3). In the PBD model, the simulation starts with the cubical element at the undeformed state. The forces are applied and the system is let evolve until the equilibrium is reached. When the velocity of the particles is below a threshold the state of the element is recorded.

The cubes considered have an edge of length 2, and are applied two sets of forces: a set of forces which cause a *small* deformation, in the order of $|\mathbf{u}_i| \simeq 0.1$ for the displaced nodes in the FEM model, and a set of forces which cause *large* deformations, of around $|\mathbf{u}_i| \simeq 0.3$. Some results for both small and large deformation tests are presented in Figure 7. The upper row corresponds to small deformations, while the lower row corresponds to large deformations. Every column corresponds to the same test under different force magnitudes. The first three columns show the shear test for $\nu = 0$, $\nu = 0.4$ and $\nu = 0.49$. The last three columns show the torsion test for the same values of the Poisson's ratio. The results for the uniaxial traction test are not shown in the figure since the difference between both cubes is very small. In general, we have observed that for small values of ν, the stiffness of the resulting PBD material is below that of the FEM model, while for high values of ν the PBD model is stiffer.

As a measure of error for the tests we have taken

$$e = \sum_{i=5}^{8} \|\mathbf{u}_i^{\text{PBD}} - \mathbf{u}_i^{\text{FEM}}\|$$

where $\mathbf{u}_i^{\text{PBD}}$ and $\mathbf{u}_i^{\text{FEM}}$ are the resulting displacements of node i for PBD and FEM respectively. In Figure 8 the relative error (defined as $e/\sum_{i=5}^{8} \|\mathbf{u}_i^{\text{FEM}}\|$) is shown for the small deformation tests at different values of ν. The relative errors for large deformation have not been represented, but they are very similar, with some values slightly smaller than the ones showed, and others slightly bigger.

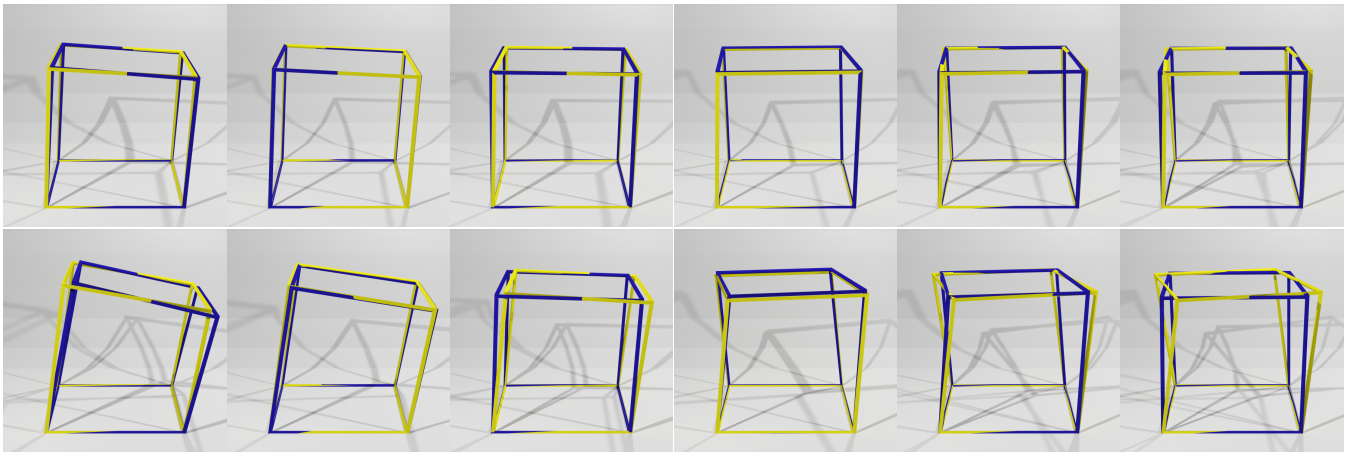

Figure 7: *Result of some deformation tests. Both cubes are presented as wireframes, with the FEM hexahedral element in yellow and the PBD cube in blue. Upper row, from left to right: small deformation for shear test, with* $\nu = 0, 0.4, 0.49$ *and torsion test for the same values of* ν*. Bottom row, from left to right: the same tests, under large deformation.*

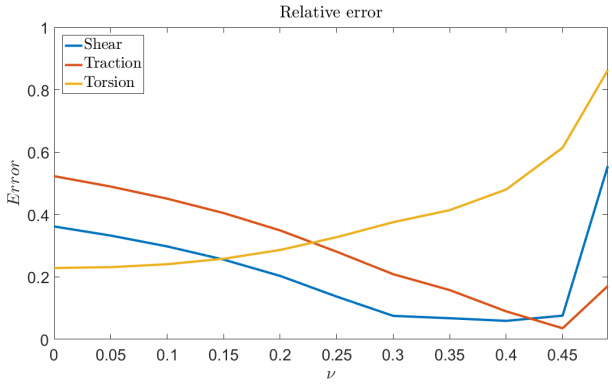

Figure 8: *Relative deformation error for a single element obtained for different values of* ν*.*

Shear and traction deformation are better approximated for the range of Poisson's ratio values where volume constraint is relevant. Error values for the shear test fall below 10% in the range $\nu \in [0.29, 0.45]$ and the error values for the traction test are below 25% for $\nu \geq 0.29$. The results indicate that the torsion test has a distinct behaviour, compared to the other two deformation modes, with an error that grows monotonously. According to the spectral analysis in [SV11], the torsion deformation is associated to the smallest nonzero eigenvalue of $\mathbf{K}^{\text{FEM}}$. Our hypothesis is that this property of FEM makes it more difficult to properly acquire the torsion behaviour, since any error in other deformation modes is more strongly penalised in the optimisation process.

5.3. Application to an hexahedral mesh

To show the behaviour of the fitted PBD model beyond a single hexahedron, we have built a $5 \times 5 \times 5$ hexahedral mesh and repeated the deformation tests. The three tests (torsion, shear, and axial deformation) have been repeated for $E = 100$ and two values of Poisson's ratio: $\nu = 0.2$ and $\nu = 0.4$. The results are shown in Figures 1, 10 and 9. Again, the material cubes simulated with PBD and FEM are superimposed in a wireframe representation. In these figures, PBD mesh is represented in green, and FEM mesh is represented in white.

The three tests for small deformation using $\nu = 0.4$ are shown in Figure 9. For both torsion and shear deformation the behaviour of the two models are quite comparable. However, in the vertical traction test the PBD material shows a much softer behaviour than the FEM material, resulting in a deformation several times larger than the reference model.

In Figure 1 torsion and shear tests are shown for $\nu = 0.2$. We observe that, in this scenario, shear deformation is much higher in PBD than in FEM, while under torsion deformation PBD remains closer to the FEM simulation. The shear deformation test is compared for two values of ν in Figure 10. This figure shows that the observation of higher error for small values of ν is also valid for the compound cube. This result indicates that PBD can serve as a good approach for the simulation of biological tissue in applications like virtual surgery, which exhibit high incompressibility values [SV11], provided that current parameter fitting limitations are overcome.

6. Conclusion

We have presented a procedure to characterise the dynamics of a PBD elastic cube, by means of the linearisation of the projection process. Our approach is based on building a stiffness matrix and seeking for the parameters that make it as close as possible, in Frobenius norm, to the equivalent stiffness matrix for linear FEM.

The analysis of the results throws several conclusions. First, the fitting by Frobenius norm has limitations since the best results give relative error around 20% during the fitting and errors over 20% in some simulation tests, depending on the value of ν. However, the

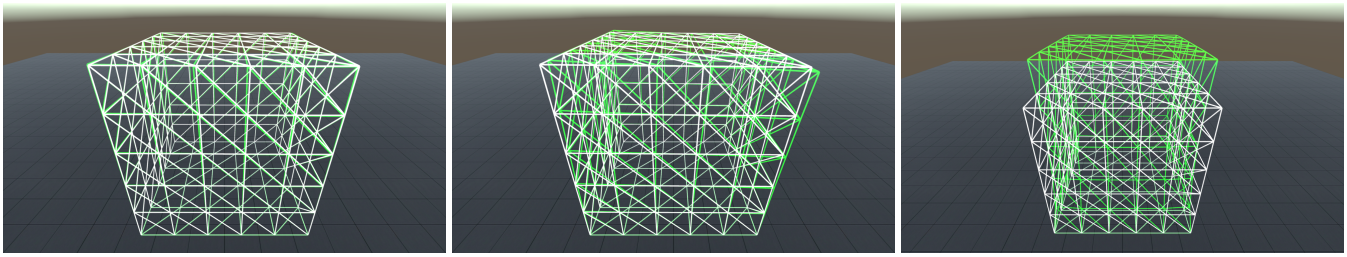

Figure 9: *Comparison between the* $5 \times 5 \times 5$ *PBD hexahedral mesh, fitted with the proposed method, and the reference FEM mesh for* $E = 100$ *and* $\nu = 0.4$*. The figures correspond (from left to right) to torsion, shear and axial deformation tests for small displacements. Green mesh corresponds to PBD and white mesh to FEM.*

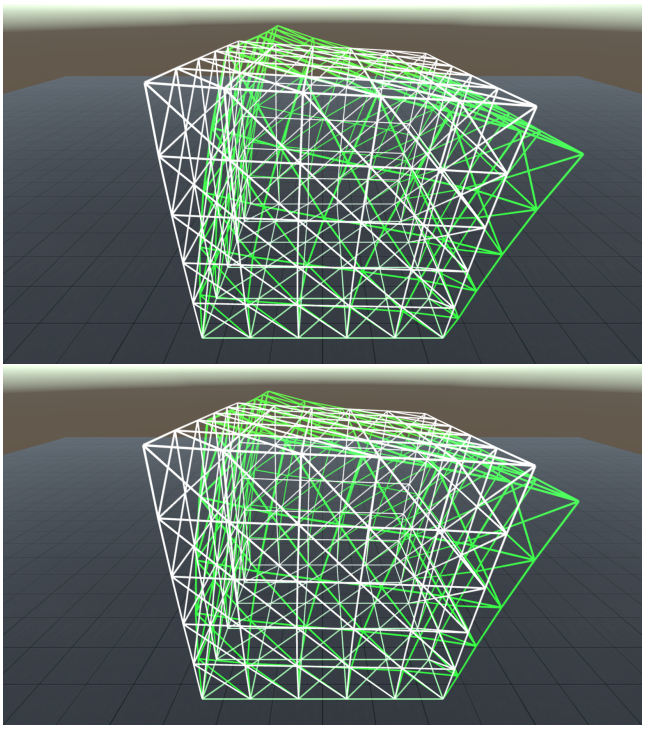

Figure 10: *Shear test for a* $5 \times 5 \times 5$ *PBD hexahedral mesh, for materials with* $\nu = 0.2$ *(top) and* $\nu = 0.4$ *(bottom). This comparison shows that better results are obtained with higher values of* ν*. Green mesh corresponds to PBD and white mesh to FEM.*

proposed procedure also shows that a systematic parameter fitting can be performed. If a proper cost function is found, PBD-based elastic models can be adjusted to reproduce certain scenarios. It is noteworthy that the best results are met for high values of Poisson's ratio, indicating that the decision to use volume constraint has been successful, specially for $\nu \geq 0.29$.

We have observed in our tests that the Frobenius norm has lead to models with lower stiffness than the reference model when the value of ν is below 0.29, while the PBD material becomes stiffer than the model over $\nu = 0.4$. These results make us think that the use of alternative fitting methods must give better results. We conjecture that a data driven approach, in which the parameters are fitted using reference samples instead of stiffness matrix, must substantially improve the results of this work. We also expect that the introduction of the number of iterations in the fitting process, which can provide stiffer behaviours with the same coefficients, will also help improve the results of the methodology.

In addition to the search of alternative fitting strategies, we consider that applying our strategy to tetrahedral meshes or bidimensional elements can also lead to interesting results. Other possible research line is the comparison to nonlinear elastic models, or the approximation of anisotropic materials. We expect that this last problem poses a hard optimisation problem, since will require the fitting of all the stiffness coefficients separately.

Acknowledgements

This research is partially funded by grant TIN2014-59932-JIN.

References

[BBJ*09] BAUDET V., BEUVE M., JAILLET F., SHARIAT B., ZARA F.: Integrating tensile parameters in mass-spring system for deformable object simulation. In *Int'l Conf. on Computer Graphics, Visalization and Computer Vision (WSCG'09)* (2009), pp. 145–152. 2

[BKCW14] BENDER J., KOSCHIER D., CHARRIER P., WEBER D.: Position-based simulation of continuous materials. *Computers & Graphics 44* (2014), 1 – 10. doi:http://dx.doi.org/10.1016/j.cag.2014.07.004. 2

[BMO*14] BENDER J., MÜLLER M., OTADUY M. A., TESCHNER M., MACKLIN M.: A survey on position-based simulation methods in computer graphics. *Computer Graphics Forum 33*, 6 (2014), 228–251. doi:10.1111/cgf.12346. 2

[BSSH04] BIANCHI G., SOLENTHALER B., SZÉKELY G., HARDERS M.: Simultaneous topology and stiffness identification for mass-spring models based on fem reference deformations. In *Medical Image Computing and Computer-Assisted Intervention Conference* (2004), pp. 293–301. doi:10.1007/978-3-540-30136-3_37. 2

[DKT95] DEUSSEN O., KOBBELT L., TIICKE P.: Using simulated annealing to obtain good nodal approximations of deformable bodies. In *Computer Animation and Simulation* (1995), pp. 30–43. 2

[EB53] ERDÉLYI A., BATEMAN H.: *Higher Transcendental Functions*, vol. 1. New York: McGraw–Hill, 1953. 3

[Gel98] GELDER A. V.: Approximate simulation of elastic membranes by triangulated spring meshes. *Journal of Graphics Tools 3*, 2 (1998), 21–41. doi:10.1080/10867651.1998.10487490. 2

[KNS15] KOT M., NAGAHASHI H., SZYMCZAK P.: Elastic moduli of simple mass spring models. *The Visual Computer 31*, 10 (2015), 1339–1350. doi:10.1007/s00371-014-1015-5. 2

[LPC95] LOUCHET J., PROVOT X., CROCHEMORE D.: Evolutionm y identification of the cloth animation m odels. In *Computer Animation and Simulation* (95), pp. 44–54. 2

[LRWW98] LAGARIAS J. C., REEDS J. A., WRIGHT M. H., WRIGHT P. E.: Convergence properties of the nelder-mead simplex method in low dimensions. *SIAM Journal of Optimization 9*, 1 (1998), 112–147. doi:10.1137/S1052623496303470. 4

[LSH07] LLOYD B., SZEKELY G., HARDERS M.: Identification of spring parameters for deformable object simulation. *IEEE Transactions on Visualization and Computer Graphics 13*, 5 (2007), 1081–1094. doi:10.1109/TVCG.2007.1055. 2, 4

[MBT03] MACIEL A., BOULIC R., THALMANN D.: Deformable tissue parameterized by properties of real biological tissue. In *Surgery Simulation and Soft Tissue Modeling* (2003), pp. 74–87. doi:10.1007/3-540-45015-7_8. 2

[MG04] MÜLLER M., GROSS M.: Interactive virtual materials. In *Proceedings of Graphics Interface* (2004), Canadian Human-Computer Communications Society School of Computer Science, University of Waterloo, Waterloo, Ontario, Canada, pp. 239–246. 1

[MHHR06] MÜLLER M., HEIDELBERGER B., HENNIX M., RATCLIFF J.: Position based dynamics. In *Proc. of 3rd workshop on Virtual Reality Interaction and Physical Simulation* (2006). 2, 3, 4

[MMCK14] MACKLIN M., MÜLLER M., CHENTANEZ N., KIM T.-Y.: Unified particle physics for real-time applications. *ACM Trans. Graph. 33*, 4 (July 2014), 153:1–153:12. doi:10.1145/2601097.2601152. 4

[NM77] NORMAN A., MOORE P.: Implementing the new risch integration algorithm. *Proceedings of the 4th International Colloquium on Advanced Computing Methods in Theoretical Physics* (1977), 99–10. 3

[NNUF04] NOGAMI R., NOBORIO H., UJIBE F., FUJII H.: Precise deformation of rheologic object under msd models with many voxels and calibrating parameters. In *Robotics and Automation, 2004. Proceedings. ICRA '04. 2004 IEEE International Conference on* (April 2004), vol. 2, pp. 1919–1926 Vol.2. doi:10.1109/ROBOT.2004.1308104. 2

[Ris69] RISCH R.: The problem of integration in finite terms. *Transactions of the American Mathematical Society*, 139 (1969), 167–189. doi:10.2307/1995313. 3

[SV11] SAN-VICENTE G.: *Designing deformable models of soft tissue for virtual surgery planning and simulation using the Mas-Spring Model*. PhD thesis, TECNUN, 2011. 2, 7

[SVAC12] SAN-VICENTE G., AGUINAGA I., CELIGUETA J. T.: Cubical mass-spring model design based on a tensile deformation test and nonlinear material model. *IEEE Transactions on Visualization and Computer Graphics 18*, 2 (2012), 228–241. doi:10.1109/TVCG.2011.32. 2, 4, 6

[THMG04] TESCHNER M., HEIDELBERGER B., MULLER M., GROSS M.: A versatile and robust model for geometrically complex deformable solids. In *Proceedings of the Computer Graphics International* (2004), pp. 312–319. doi:10.1109/CGI.2004.6. 4

[ZGF07] ZERBATO D., GALVAN S., FIORINI P.: Calibration of mass spring models for organ simulations. In *IEEE Intl. Conference on Intelligent Robots and Systems* (2007), pp. 370–375. 2

[Zie77] ZIENKIEWICZ O. C.: *The finite element method*, 3rd ed. London : McGraw-Hill, 1977. 3